Enhanced frequency-adaptive self-tuning filter-based continuous terminal sliding mode control of single-phase dynamic voltage restorer

Ahmed, Hafiz; Biricik, Samet; Komurcugil, Hasan; Elghali, Seifeddine Ben ; Benbouzid, Mohamed

IFAC Control Engineering Practice

DOI:
https://doi.org/10.1016/j.conengprac.2022.105340

E-pub ahead of print: 01/11/2022

Publisher's PDF, also known as Version of record

Control Engineering Practice 128 (2022) 105340

Contents lists available at ScienceDirect

Control Engineering Practice

journal homepage: www.elsevier.com/locate/conengprac

Enhanced frequency-adaptive self-tuning filter-based continuous terminal sliding mode control of single-phase dynamic voltage restorer☆

Hafiz Ahmed [a,*], Samet Biricik [b], Hasan Komurcugil [c], Seifeddine Ben Elghali [d], Mohamed Benbouzid [e,f]

[a] Nuclear Futures Institute, Bangor University, Bangor LU57 1UT, United Kingdom
[b] Department of Electrical and Electronic Engineering, European University of Lefke, Lefke 99728, Turkey
[c] Department of Computer Engineering, Eastern Mediterranean University, 99628 Famagusta, Via Mersin 10, Turkey
[d] Aix-Marseille University, UMR CNRS 7020 LIS, Marseille, France
[e] University of Brest, UMR CNRS 6027 IRDL, 29238 Brest, France
[f] Shanghai Maritime University, 201306 Shanghai, China

ARTICLE INFO

Keywords:
Dynamic voltage restorer
Voltage sag
Voltage swell
Voltage harmonics
Self-tuning filter
Continuous sliding mode control

ABSTRACT

This paper presents a continuous terminal sliding mode controller (CTSMC) for single-phase dynamic voltage restorers (DVRs). The presented controller can substantially eliminate the chattering compared to the first-order sliding mode counterpart while achieving faster convergence speed compared to the super twisting counterpart. Moreover, the continuous control signal enables the voltage source inverter to operate at constant switching frequency. As the reference compensation voltage generator, an enhanced single-phase self-tuning (SP-STF) filter is also proposed. The SP-STF has excellent band-pass filtering property, can completely attenuate DC offset and has fast dynamic response. The SP-STF has been made frequency-adaptive through unknown grid frequency estimation under a delayed-based linear regression framework. Comprehensive stability analysis of the controller and filter are presented. Experimental studies are performed to demonstrate the effectiveness of the proposed comprehensive control solution. Comparative simulation studies are also provided to highlight the advantages of the proposed approach. Results show that the proposed technique can quickly detect and compensate for any grid voltage fluctuations and helps to maintain constant voltage at the load side despite voltage sag/swell and distortions.

1. Introduction

Power quality is very important to ensure smooth operation of the electric power system (Ahmed, 2015; Çelik, 2022; Çelik & Meral, 2019; Malathi & Jayachandran, 2020). Electric power fluctuations (flickers) may interrupt the operation of some critical devices used in hospitals, factories, base stations of cellular networks, homes, and IT sector. Generally, these fluctuations exist in the utility grid in the form of voltage sag (voltage dip), voltage swell, and harmonic distortions. In order to protect these devices from such fluctuations, custom power devices known as dynamic voltage restorers (DVRs) have been developed (Moghassemi & Padmanaban, 2020). Basic DVR topology consists of a dc voltage source (energy storage), a voltage source inverter, an LC filter, and a transformer whose secondary winding is connected between the grid and the load in series. The main function of a DVR is to inject a compensation voltage into the point of common coupling, such that the voltage fluctuations existing in the grid do not affect the voltage which feeds critical devices. In other words, the input voltage of the critical devices (from now on, it will be called the load voltage) always remains unchanged, regardless of the voltage fluctuations in the grid.

In order to design a DVR which fulfills the desired operation, the voltage fluctuations should be first detected. Voltage sag occurs when there is a momentary decrease in the nominal grid voltage (IEEE Recommended Practice for Evaluating Electric Power System Compatibility With Electronic Process Equipment, 1998). Generally, the voltage sags occur due to the short circuit faults in the grid such as sudden load connections, startup of induction motors with high ratings, and ground faults in the power system. On the other hand, voltage swell happens when there is a momentary increase in the nominal grid voltage (IEEE Recommended Practice for Evaluating Electric Power System Compatibility With Electronic Process Equipment, 1998). Voltage swell occurs

☆ The work of H. Ahmed is supported by the Sêr Cymru II 80761-BU-103 project by Welsh European Funding Office (WEFO) under the European Regional Development Fund (ERDF).

* Corresponding author.
E-mail address: hafiz.h.ahmed@ieee.org (H. Ahmed).

https://doi.org/10.1016/j.conengprac.2022.105340
Received 21 April 2022; Received in revised form 20 July 2022; Accepted 27 August 2022
Available online xxxx

when a large load is disconnected and large capacitors are switched on. The duration of voltage sags and voltage swells varies from 0.5 cycles to one minute maximum. For this reason, these voltage fluctuations should be detected and compensated very quickly. In the ideal case, detection of voltage sag/swell is relatively easy. However, the presence of harmonics in the grid voltage makes it difficult to develop an effective voltage fluctuation strategy. If the reference voltage estimation method is not harmonically robust, this will increase the overall total harmonic distortion. This will increase the loss and reduce the efficiency.

The speed of detection and compensation is determined by the method used to control the DVR. The control method also determines the quality of the load voltage. In order to improve the power quality through DVR, there are two main challenges. Firstly, the control method needs to detect the deviation in grid voltage amplitude from the nominal value using noisy and potentially harmonically distorted grid voltage measurement. This necessitates the development of an advanced grid frequency-adaptive filtering technique to filter the measured grid voltage, which is used to compute the necessary compensation voltage reference. Secondly, the control methods need to track the reference compensation voltage in a quick manner while reducing the total harmonic distortion of the load voltage. This necessitates the development of a robust control method that can deal with external disturbances and parametric uncertainties while at the same time providing fast convergence. These are the key control challenges for DVR.

So far, many control methods and DVR topologies have been developed by the researchers to meet the required control objectives and challenges. These control methods include proportional–integral (PI) (including evolutionary optimization-based control parameter tuning) (Omar, Aleem, El-Zahab, Algablawy, & Ali, 2019), state feedback (Kim & Sul, 2005), H_∞ control (Li, Blaabjerg, Vilathgamuwa, & Loh, 2007), repetitive control (Roncero-Sánchez, Acha, Ortega-Calderon, Feliu, & García-Cerrada, 2008), hysteresis control (Sasitharan & Mishra, 2010), fuzzy logic control (Roselyn et al., 2020), and sliding mode control (SMC) (Biricik & Komurcugil, 2016; Biricik, Komurcugil, Tuyen, & Basu, 2019; Komurcugil, Biricik, Bayhan, & Zhang, 2021), to name a few. Conventionally, the PI controller in the synchronous frame (SRF) is the most widely used control method for three-phase DVR. However, the application of SRF-PI is not straightforward for a single-phase system. It requires the implementation of quadrature signal generators which add implementation and tuning complexity. Moreover, current sensors are also required which limits the choice of micro-controllers with built-in analog sensor signal processing capability. The main drawback of the state feedback control is its intensive computation requirement in generating the compensation voltage reference. Even though the H_∞ control has strong robustness, it suffers from implementation complexity. The repetitive control is quite successful in eliminating the periodic disturbances. However, its performance under non-periodic disturbances is not satisfactory. Hysteresis control is also characterized by robustness against parameter variations with fixed switching frequency. However, the inverter should be operated with high switching frequency so as to achieve the desired compensation performance. The problem with fuzzy logic control is the lack of systematic design procedure. The number and shape of membership functions are selected by trial-and-error method. The SMC method offers many advantages such as fast dynamic response, simple implementation, and insensitivity to parameter variations (Falehi & Torkaman, 2021; Pandey, Agrawal, Mandloi, & Sarkar, 2017; Toumi et al., 2020). The SMC method has been widely adopted for controlling power and energy systems, especially microgrids (Ding, Han, & Ning, 2022; Ding, Han, Ning, & Yue, 2020; Ning, Han, & Ding, 2020, 2021). DVR is a popular solution to improve the power quality issues of microgrids. In the case of single-phase DVR, SMC methods can be used using voltage sensors only which results in cost reduction and reliability enhancement of the complete system. However, it suffers from chattering phenomenon (Biricik & Komurcugil, 2016; Biricik et al., 2019). In Biricik, Komurcugil, Ahmed, and Babaei (2021), Ouchen, Benbouzid, Blaabjerg, Betka, and Steinhart (2021), it is shown that the chattering can be reduced by the super twisting algorithm based on SMC. Super twisting algorithm has the chattering reduction capability whereas terminal sliding mode control has fast convergence property. To take the benefit of the both world, in recent time, continuous terminal sliding mode control (CTSMC) has been proposed in the literature (Fridman, Moreno, Bandyopadhyay, Kamal, & Chalanga, 2015). CTSMC has fast convergence, generates continuous control signals and achieves better sliding accuracy than the super twisting or terminal sliding mode control alone. This motivated the selection of CTSMC as the control method.

Generating the reference voltage is an integral part of the DVR control system. In the ideal case, generating the reference voltage from the measured grid voltage is straightforward. However, practical grid voltage often contains harmonics. Moreover, the frequency is also fluctuating around the nominal value. These issues complicate the reference voltage generation. To overcome this issue, phase-locked loop (PLL) has widely been adopted in the DVR control literature (Hafezi & Faranda, 2017; Kumar & Mishra, 2015; Trabelsi, Komurcugil, Refaat, & Abu-Rub, 2018). In the single-phase case, PLL needs a quadrature signal generator (QSG). For this purpose, quarter-delay (T/4) is a popular approach. However, in the non-ideal grid frequency case, the delay can be fractional. Moreover, if fixed delay is used, then additional compensation mechanisms need to be considered. This complicates the design process. Some other methods of generating the quadrature signals are: second-order generalized integrator (SOGI) (Ahmed & Benbouzid, 2020b; Al Hosani, Nguyen, & Al Sayari, 2018; Rodríguez et al., 2011; Singh & Jain, 2019; Vamja & Mulla, 2022), adaptive notch filter (Biricik et al., 2019), all-pass filter (Gautam, Xiao, Lu, Ahmed, & Guerrero, 2022), Lyapunov estimator (Ahmed & Benbouzid, 2020a; Verma, Subramanian, & Jarial, 2022) and Luenberger observer (Ahmed, Pay, Benbouzid, Amirat, & Elbouchikhi, 2020; Pay, Cao, Sun, & McCluskey, 2020). In recent times, self-tuning filter (STF) became very popular in the literature as a filtering technique for DVR controller (Abdusalam, Poure, Karimi, & Saadate, 2009; Biricik, Khadem, Redif, & Basu, 2018; Chedjara et al., 2018; Safa, Berkouk, Messlem, Chedjara, & Gouichiche, 2018). STF has excellent dynamic performance and provides band-pass filtering property which can be very beneficial to extract the fundamental component from the distorted grid voltage signals. However, it is only applicable for three-phase systems. This issue has been avoided in Biricik, Redif, Özerdem, Khadem, and Basu (2014) by using T/4 delay-based QSG. As discussed previously, this approach can introduce estimation error in the non-ideal grid due to the grid frequency fluctuations. Moreover, STF is also sensitive to the presence of DC offset in the measurement. In this paper, we propose a novel STF for a single-phase system without using any delay. The proposed single-phase STF (SP-STF) has a similar frequency domain property as that of the standard STF applicable for three-phase systems. Moreover, a pre-loop filter is also proposed to further enhance the filtering property. Thanks to the pre-loop filter, the proposed SP-STF is also robust to any potential DC offset in the measured voltage signal. To make the SP-STF frequency-adaptive, delay-based linear regression framework (Ahmed, Ushirobira, & Efimov, 2021, 2022) is considered. An advantage of this approach is that the frequency estimation is decoupled from the filtering stage which makes the overall system linear and the closed-loop system fast responsive. Moreover, excellent harmonic robustness is an added advantage.

Contributions of this work are twofold. Firstly, a continuous terminal sliding mode control strategy is applied for the first time to single-phase DVR. The applied control scheme can reduce the chattering and at the same time has fast dynamic response compared to conventional sliding mode controller such as super twisting sliding mode control (ST-SMC) (Biricik et al., 2021). Numerical simulation results are provided to support this claim. Secondly, to generate the reference compensation voltage for the proposed controller, a frequency-adaptive single-phase

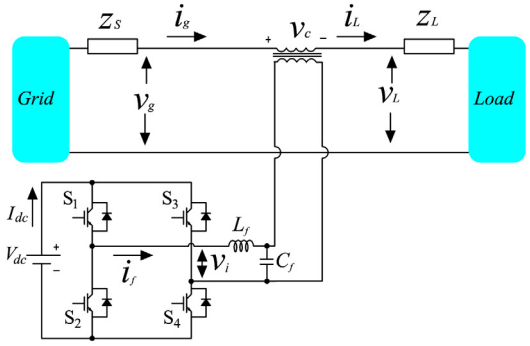

Fig. 1. Schematic of the DVR-connected system.

enhanced self-tuning filter is also developed. The developed filter has excellent filtering and DC offset rejection capability. It has better harmonic filtering capability compared to existing methods such as SOGI frequency locked-loop (SOGI-FLL) (Rodríguez et al., 2011). Comparative numerical simulation and experimental results are provided to validate the effectiveness of the developed filters in reducing the total harmonic distortion.

This paper is organized as follows: Section 2 gives an overview of the modeling and operation principle of the DVR. Details of the control and filtering techniques being developed in this work are given in Section 3. Comprehensive numerical simulation and experimental results are given in Section 4. Comparative studies are presented in Section 5. Finally, Section 6 concludes this paper.

2. Problem formulation

The considered single-phase DVR topology is given in Fig. 1. In this system, an H-bridge voltage source inverter is connected in series with a transformer to the sensitive load that is being protected. The transformer provides galvanic isolation between the DVR and the load. The DVR continuously monitors the grid voltage $v_g(t)$ (with grid impedance z_s) and injects the necessary compensation voltage to maintain the constant voltage at the load end. Differential equations governing the dynamics of the DVR are given by:

$$L_f \frac{di_f}{dt} = v_i - v_c, \tag{1}$$

$$C_f \frac{dv_c}{dt} = i_f - i_g, \tag{2}$$

where filter inductor and capacitor are denoted by L_f and C_f, filter and grid currents are denoted by i_f and i_g, compensation voltage is denoted by v_c, and the output voltage of the H-bridge inverter is denoted by $v_i = uV_{dc}$ with V_{dc} being the DC-link voltage and u is the control input. The compensation voltage is directly related to the grid and load voltages and given by:

$$v_c(t) = v_g(t) - V_L(t), \tag{3}$$

where $V_L(t)$ is the load voltage. In the ideal case i.e. disturbance-free grid case, the load voltage will be the same as the grid voltage. In this case, the compensation voltage will be zero. However, in the presence of various disturbances such as voltage sag/swell, harmonics etc., the DVR control system needs to generate the ideal reference compensation voltage and force the DVR to follow the reference compensation voltage to maintain desired voltage at the load side. To facilitate the control design, let us assume that the reference compensation voltage is given by $v_c^\star$. Then, the compensation voltage error and its derivative are given by:

$$\bar{v}_c = v_c - v_c^\star, \tag{4}$$

$$\tilde{v}_c = \dot{\bar{v}}_c = \dot{v}_c - \dot{v}_c^\star. \tag{5}$$

Then, with respect to state variables $\bar{v}_c$ and $\tilde{v}_c$, the estimation error dynamics are given by:

$$\dot{\bar{v}}_c = \tilde{v}_c, \tag{6}$$

$$\dot{\tilde{v}}_c = -\alpha\bar{v}_c + \alpha u V_{dc} + \varpi(t), \tag{7}$$

where $\alpha = 1/L_f C_f$ and the lumped unknown disturbance term is given by:

$$\varpi(t) = -\frac{1}{C_f}\frac{di_g}{dt} - \alpha v_c^\star - \dot{v}_c^\star. \tag{8}$$

We assume that the unknown disturbance term is uniformly bounded and Lipschitz continuous i.e. $|\varkappa| = |\frac{d\varpi}{dt}| < \varpi^+$, where ϖ^+ is a known positive constant.

The control problem considered in this work is to design a suitable u that will ensure that the compensation error $\bar{v}_c$ converges to zero despite the presence of the disturbance term $\varpi(t)$.

3. Proposed solution

3.1. Continuous sliding mode controller development

To design the controller u for the error system (6)–(7), we will consider the Continuous Terminal Sliding Mode (CTSM) approach proposed in Fridman et al. (2015). CTSM is a combination of two high order sliding mode (HOSM) approaches, namely the super twisting algorithm and the continuous terminal sliding mode algorithm. This helps to substantially eliminate the chattering phenomenon and gives continuous control signals. For this purpose, let us consider the following sliding surface:

$$\sigma = \tilde{v}_c + \lambda_2 \lceil \bar{v}_c \rfloor^{\frac{2}{3}}, \lambda_2 > 0, \tag{9}$$

where $\lceil \beta \rfloor^\eta = |\beta|^\eta \text{sign}(\beta)$, for any non-negative real number η. Considering the sliding surface σ, the CTSM control signal is given by:

$$u = \frac{1}{\alpha V_{dc}}\left(\alpha\tilde{v}_c - \lambda_1 \lceil \sigma \rfloor^{\frac{1}{2}} + \tilde{u}\right), \lambda_1 > 0, \tag{10}$$

$$\dot{\tilde{u}} = -\lambda_3 \int_0^t \lceil \sigma \rfloor^0 d\tau, \lambda_3 > 0. \tag{11}$$

The positive constants λ_1, λ_2 and λ_3 are suitably designed control gains. For further analysis, we assume that in addition to the compensation error $\bar{v}_c$, its derivative $\tilde{v}_c$ is also available. If it is not readily available, then a second-order sliding mode differentiator can be implemented (Ahmed, Ríos, Ayalew, & Wang, 2018). Out of various choices available in the literature, the following uniform robust exact differentiator (Cruz-Zavala, Moreno, & Fridman, 2011) with fixed-time convergence property can be considered:

$$\dot{\hat{\tilde{v}}}_c = -\xi_1\left(\left\lceil \hat{\bar{v}}_c - \bar{v}_c \right\rfloor^{\frac{1}{2}} + \xi_2 \left\lceil \hat{\bar{v}}_c - \bar{v}_c \right\rfloor^{\frac{3}{2}}\right) + \tilde{v}_c, \tag{12}$$

$$\dot{\hat{\bar{v}}}_c = -\xi_3\left(\frac{1}{2}\left\lceil \hat{\bar{v}}_c - \bar{v}_c \right\rfloor^0 + 2\xi_2\left(\hat{\bar{v}}_c - \bar{v}_c\right) + \frac{3}{2}\xi_2^2\left\lceil \hat{\bar{v}}_c - \bar{v}_c \right\rfloor^2\right), \tag{13}$$

where $\hat{\cdot}$ indicates estimated value, $\xi_1, \xi_3 > 0$ are tuning gain and $\xi_2 \geq 0$ is a scalar gain. For the sake of implementation and analysis simplicity, we assume that full state measurements are available.

To analyze the stability of the presented control technique, let us substitute the control (10)–(11) into the error system (6)–(7). Then, the following can be obtained:

$$\dot{\bar{v}}_c = \tilde{v}_c, \tag{14}$$

$$\dot{\tilde{v}}_c = -\lambda_1 \lceil \sigma \rfloor^{\frac{1}{2}} + \tilde{u} + \varpi, \tag{15}$$

$$\dot{\tilde{u}} = -\lambda_3 \lceil \sigma \rfloor^0. \tag{16}$$

Let us consider that $\tilde{\bar{v}}_c = \tilde{u} + \varpi$. Then, the Eqs. (14)–(16) can be rewritten as:

$$\dot{\tilde{\bar{v}}}_c = \tilde{v}_c, \tag{17}$$

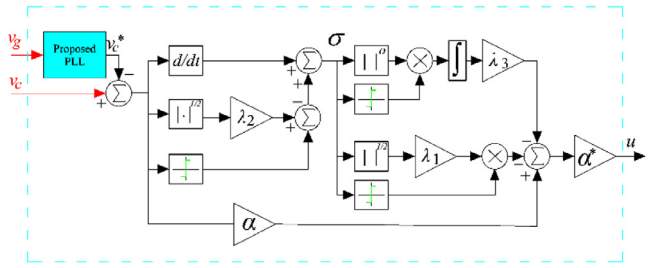

Fig. 2. Block diagram of the CSTSM controller.

$$\dot{\tilde{v}}_c = -\lambda_1 \lceil \sigma \rfloor^{\frac{1}{2}} + \tilde{\tilde{v}}_c, \tag{18}$$

$$\dot{\tilde{\tilde{v}}}_c = -\lambda_3 \lceil \sigma \rfloor^{0} + \varkappa, \tag{19}$$

where $\varkappa$ is the derivative of the lumped disturbance term ϖ and satisfies $|\varkappa| \leq \varpi^+$ as assumed in the problem formulation given in Section 2. Closed-loop error system (17)–(19) mimics the CSTSM algorithm in Fridman et al. (2015).

To analyze the stability of the CSTSM controller as applied to the DVR system, let us consider the following quadratic Lyapunov function (Fridman et al., 2015):

$$V = \Pi^T \Phi \Pi, \tag{20}$$

where $\Pi = [\lceil \tilde{v}_c \rfloor^{\frac{2}{3}} \ \sigma \ \lceil \tilde{\tilde{v}}_c \rfloor^{2}]^T$ and

$$\Phi = \begin{bmatrix} \phi_1 & -\frac{1}{2}\phi_{12} & \frac{1}{2}\phi_{13} \\ -\frac{1}{2}\phi_{12} & \phi_2 & -\frac{1}{2}\phi_{23} \\ \frac{1}{2}\phi_{13} & -\frac{1}{2}\phi_{23} & \phi_3 \end{bmatrix},$$

where the elements of the matrix Φ are suitably selected to ensure that the Lyapunov function (20) is positive definite and radially unbounded. If the parameters are chosen as $\lambda_1 > \lambda_2 > \lambda_3 > \varpi^+$, then it has been shown in Fridman et al. (2015) that $\dot{V} \leq -\kappa V^{\frac{3}{4}}$ for some positive constant κ. This shows the finite-time stability of the closed-loop error system (17)–(19). This implies finite-time convergence of the compensation voltage tracking error. Block diagram of the CSTSM controller is given in Fig. 2.

3.2. Reference voltage generation

The controller presented in Section 3.1 requires the reference compensation voltage $v_c^\star$. For this purpose, let us consider the single-phase grid voltage $v_g(t)$ given by:

$$v_g(t) = V_{g0} + V_g \sin(\omega t + \varphi), \tag{21}$$

where V_{g0} is the DC offset, V_g is the magnitude, ω is the angular frequency, φ is the phase angle and the instantaneous phase is given by $\theta = \omega t + \varphi$. The grid frequency ω is unknown but has a known nominal value $\omega_n = 100\pi$. In the ideal case and without DC offset, the reference load voltage can be generated by:

$$V_L^\star = \mu \frac{v_g}{V_g} = \mu \sin(\theta), \tag{22}$$

where μ is the desired magnitude of the reference current. From $V_L^\star$, the reference compensation voltage can be calculated as:

$$v_c^\star = v_g - V_L^\star. \tag{23}$$

In the ideal case i.e. disturbance-free grid, generating $V_L^\star$ and consequently $v_c^\star$ is straightforward. However, in practice, the grid voltage magnitude is not constant and can have voltage sag/swell. Moreover, harmonics, especially lower order ones, are often present. In this case, extracting the instantaneous phase θ from the disturbed grid voltage v_g is required. For this purpose, a self-tuning filter (STF) framework will be considered in this work.

STF (Abdusalam et al., 2009; Biricik et al., 2018, 2014; Chedjara et al., 2018; Safa et al., 2018) is originally proposed for the three-phase system working in the stationary reference frame. It has excellent filtering properties and can extract the fundamental component from very noisy measured signals. The transfer function of STF is given by:

$$\frac{V_{xy}}{U_{xy}}(s) = Y \frac{(s + j\omega)}{(s + Y)^2 + \omega^2}, Y > 0, \tag{24}$$

where Y is the tuning parameter, U_{xy} and V_{xy} are the filter input and output phasor signals. From the transfer function, it is clear that STF is a band-pass filter. The STF filter cannot be applied directly to the single-phase system as only one measurement signal is available. To overcome this limitation, fixed time-delay based quadrature signal is generated in Biricik et al. (2014) to make STF suitable for single-phase systems. However, in the actual power grid, the frequency is not constant. As such, fixed time-delay based quadrature signal generation may introduce estimation error under frequency fluctuation. A potential solution could be the use of frequency adaptive time-delay. However, this may introduce fractional time-delay and implementing fractional delay is computationally expensive. To overcome this issue, in this work, STF-type filters will be used to generate the quadrature signal. For further consideration, this filter will be named as Single-Phase STF (SP-STF).

To facilitate the design of the SP-STF, let us consider the following state variables:

$$\zeta_1 = -V_g \cos(\theta), \tag{25}$$

$$\zeta_2 = V_g \sin(\theta), \tag{26}$$

where ζ_2 is the measured grid voltage and ζ_1 is the quadrature signal of ζ_1. Then, the dynamics of the grid voltage signal without the DC offset is given by:

$$\dot{\zeta}_1 = \omega \zeta_2, \tag{27}$$

$$\dot{\zeta}_2 = -\omega \zeta_1. \tag{28}$$

The issue of DC offset will be addressed in Section 3.2.3. For system (27)–(28), the following SP-STF can be designed:

$$\dot{\hat{\zeta}}_1 = \hat{\omega} \hat{\zeta}_2, \tag{29}$$

$$\dot{\hat{\zeta}}_2 = -\hat{\omega} \hat{\zeta}_1 + \lambda_4 \left(\zeta_2 - \hat{\zeta}_2 \right), \tag{30}$$

where $\hat{}$ represents estimated value and λ_4 is the tuning parameter. In Eqs. (29) and (30), estimated grid frequency is used. Details of the frequency estimation will be given in Section 3.2.1. To demonstrate the similarity of SP-STF and STF, let us consider the following transfer functions of the SP-STF:

$$\frac{\hat{\zeta}_1}{\zeta_2}(s) = G_1(s) = \frac{\lambda_4 \hat{\omega}}{s^2 + \lambda_4 s + \hat{\omega}^2}, \tag{31}$$

$$\frac{\hat{\zeta}_2}{\zeta_2}(s) = G_2(s) = \frac{\lambda_4 s}{s^2 + \lambda_4 s + \hat{\omega}^2}. \tag{32}$$

Then, in the phasor form i.e. $G_3(s) = G_2(s) + jG_1(s)$, SP-STF transfer function is given by:

$$G_3(s) = \lambda_4 \frac{s + j\hat{\omega}}{s^2 + \lambda_4 s + \hat{\omega}^2}. \tag{33}$$

Transfer functions (24) and (33) show that the original STF and the proposed single-phase version both act as a band-pass filter. This shows the similarity between the two filters. It is to be noted here that the proposed SP-STF has some structural similarity with the well known second-order generalized integrator (SOGI) (Dao, Biricik, & Ngo, 2020; Mukundan C. M., Naqvi, Singh, & Jayaprakash, 2021; Nirmal Mukundan, Naqvi, Singh, Singh, & Jayaprakash, 2021). The feedback term in SP-STF is frequency independent whereas the feedback term in SOGI is frequency dependent. As such, we need one multiplication operation less than SOGI which reduces the computational complexity. Moreover, transfer functions (31) and (32) of SP-STF are also different from SOGI transfer functions.

3.2.1. Grid frequency estimation

The developed SP-STF requires estimated grid frequency for frequency-adaptive operation of the filter. This issue is going to be addressed in this Section. For the development of frequency estimator, let us consider the following delayed versions on the grid voltage signal (21) with $v_g^{l\tau} = v_g(t - l\tau), l = 1, 2, 3$:

$$v_g^{\tau} = V_{g0} + V_g \sin(\theta)\cos(\omega\tau) - V_g \cos(\theta)\sin(\omega\tau), \tag{34}$$

$$v_g^{2\tau} = V_{g0} + V_g \sin(\theta)\cos(2\omega\tau) - V_g \cos(\theta)\sin(2\omega\tau), \tag{35}$$

$$v_g^{3\tau} = V_{g0} + V_g \sin(\theta)\cos(3\omega\tau) - V_g \cos(\theta)\sin(3\omega\tau). \tag{36}$$

Using (21) and (34)–(36), one can obtain that:

$$\begin{aligned}(v_g^{2\tau} - v_g^{\tau})(1 + 2\cos(\omega\tau)) &= -V_g(\sin(\theta) - \sin(\theta - 3\omega\tau)),\\ &= v_g^{3\tau} - v_g.\end{aligned} \tag{37}$$

Eq. (37) can be organized as:

$$v_g - v_g^{\tau} + v_g^{2\tau} - v_g^{3\tau} = 2(v_g - v_g^{2\tau})\cos(\omega\tau). \tag{38}$$

Eq. (38) can be written as a first-order regression model:

$$y = X\beta, \tag{39}$$

where $y = v_g - v_g^{\tau} + v_g^{2\tau} - v_g^{3\tau}$, $X = 2(v_g^{\tau} - v_g^{2\tau})$, and $\beta = 2\cos(\omega\tau)$. The unknown parameter β can easily be estimated from Eq. (39) by applying linear regression and given below :

$$\dot{\hat{\beta}} = \lambda_5 X(y - X\hat{\beta}), \tag{40}$$

where the positive parameter λ_5 controls the convergence rate. From the estimated unknown parameter $\hat{\beta}$, the actual grid frequency can be evaluated as:

$$\hat{\omega} = \arccos(\beta)/\tau.$$

To analyze the stability of the estimator (40), let us consider the unknown parameter estimation error as $\tilde{\beta} = \beta - \hat{\beta}$. Then, the error dynamics is given by:

$$\dot{\tilde{\beta}} = -\lambda_5 X^2 \tilde{\beta}. \tag{41}$$

Solution of Eq. (41) is given by:

$$\tilde{\beta}(t) = e^{-\lambda_5 \int_0^t X^2(\tau)d\tau}\tilde{\beta}(0). \tag{42}$$

The error will converge to zero exponentially if X is bounded. For any $\tau < \pi/\omega$, X is bounded which makes the unknown parameter estimation error exponentially stable.

The unknown frequency estimator has two gains to be tuned, delay τ and control gain λ_5. Through extensive numerical simulation, it has been found that $\tau = T/4$ can be a good choice where T is the fundamental period of the grid voltage. Control gain λ_5 has to be tuned as a compromise between fast dynamic response and disturbance rejection capability.

3.2.2. Stability analysis of SP-STF

To analyze the stability of the SP-STF, let us consider $r^2 = \hat{\zeta}_1^2 + \zeta_2^2$ and $\hat{\theta} = \text{atan}(\hat{\zeta}_2/\hat{\zeta}_1)$ with $\hat{\zeta}_1 = r\cos(\hat{\theta})$ and $\hat{\zeta}_2 = r\sin(\hat{\theta})$. Then, the SP-STF (29)–(30) in polar coordinates can be written as:

$$\dot{r} = \lambda_4 r \sin(\hat{\theta})\tilde{y}_{\zeta}, \tag{43}$$

$$\dot{\hat{\theta}} = -\hat{\omega} + \lambda_4 r^{-1}\cos(\hat{\theta})\tilde{y}_{\zeta}, \tag{44}$$

where $\tilde{y}_{\zeta} = \zeta_2 - \hat{\zeta}_2$. Let us consider the synchronization error i.e. error between the actual the estimated instantaneous phase of the grid as:

$$\tilde{\theta} = \theta - \hat{\theta}. \tag{45}$$

With respect to the synchronization error, the closed-loop SP-STF in polar coordinates (43)–(44) can be rewritten as:

$$\dot{r} = \lambda_4 r \sin\left(\theta - \tilde{\theta}\right)\tilde{y}_{\zeta}, \tag{46}$$

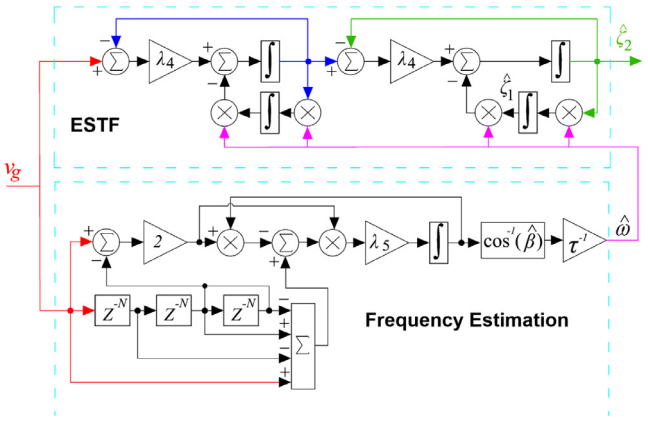

Fig. 3. Block diagram of the proposed enhanced STF based grid-synchronization technique.

$$\dot{\tilde{\theta}} = \hat{\omega} - \omega - \lambda_4 r^{-1}\cos(\theta - \tilde{\theta})\tilde{y}_{\zeta}, \tag{47}$$

where $\tilde{y}_{\zeta} = V_g \sin(\theta) - r\sin(\theta - \tilde{\theta})$. System (46)–(47) has the following equilibrium point:

$$\Xi^{\star} = \{r = V_g, \tilde{\theta} = 0\}. \tag{48}$$

Jacobian of the system (46)–(47) with respect to the equilibrium point (48) is given by:

$$J\left(\Xi^{\star}\right) = \begin{bmatrix} -V_g\lambda_4\sin^2(\theta) & 0.5V_g^2\lambda_4\sin(2\theta) \\ \lambda_4\sin(2\theta)/(2V_g) & -\lambda_4\cos^2(\theta) \end{bmatrix}. \tag{49}$$

Stability of the Jacobian matrix (49) can be obtained through the following characteristics polynomial:

$$s^2 + \{\lambda_4\cos^2(\theta) + V_g\lambda_4\sin^2(\theta)\}s = 0. \tag{50}$$

A stable second-order polynomial has all non-negative coefficients. Since, all coefficients are non-negative, local-stability of SP-STF is ensured.

3.2.3. Enhanced SP-STF

The proposed SP-STF is designed by assuming an ideal grid. In practice, various abnormalities such as harmonics, DC offset may be present. In this case, estimation error is inevitable. To overcome this limitation, a pre-loop filter can be very useful. For further consideration, pre-loop filter enabled SP-STF will be named as enhanced STF (ESTF). The block diagram of the ESTF is given in Fig. 3. In ESTF, two SP-STFs are used. The first one works as the pre-loop filter while the second one is used for estimating the unknown frequency. The pre-loop filter can remove any DC offset.

Transfer functions of the ESTF are given by:

$$\frac{\hat{\zeta}_1}{\zeta_2}(s) = \frac{\lambda_4^2\hat{\omega}s}{\left(s^2 + \lambda_4 s + \hat{\omega}\right)^2}, \tag{51}$$

$$\frac{\hat{\zeta}_1}{\zeta_2}(s) = \frac{\lambda_4 s^2}{\left(s^2 + \lambda_4 s + \hat{\omega}\right)^2}. \tag{52}$$

Bode magnitude plot for the transfer functions (31) and (51) i.e. for the quadrature signal are given in Fig. 4. This figure shows that ESTF blocks the DC offset as the gain is zero for $s = 0$. This is not true for SP-STF. Moreover, for high frequency cases, SP-STF has a decay rate of −40 dB/Decade whereas ESTF has a decay rate of −60 dB/Decade. This shows 1.5 times better filtering property. Similar, excellent performance can be seen for the direct signal also. In this case, the Bode magnitude plot for the transfer functions (32) and (52) are given in Fig. 5. In the high frequency case, ESTFs decay rate is −40 dB/Decade which is two times faster than STF. As a result, ESTF can be considered

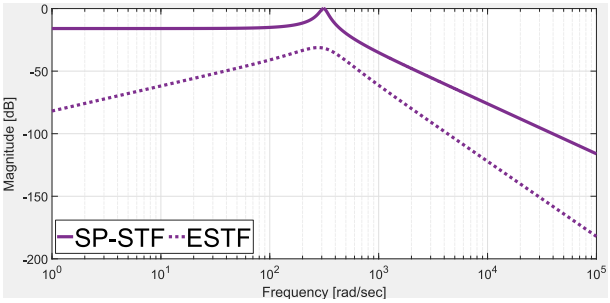

Fig. 4. Bode magnitude plot for transfer functions (31) and (51) with $\lambda_4 = 50$.

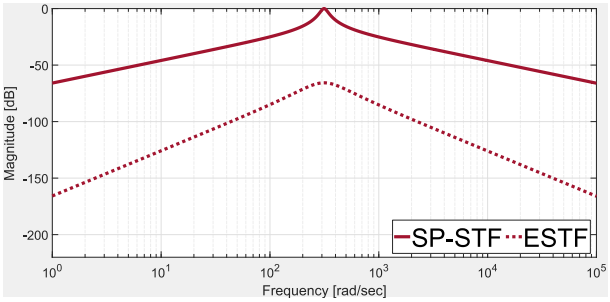

Fig. 5. Bode magnitude plot for transfer functions (32) and (52) with $\lambda_4 = 50$.

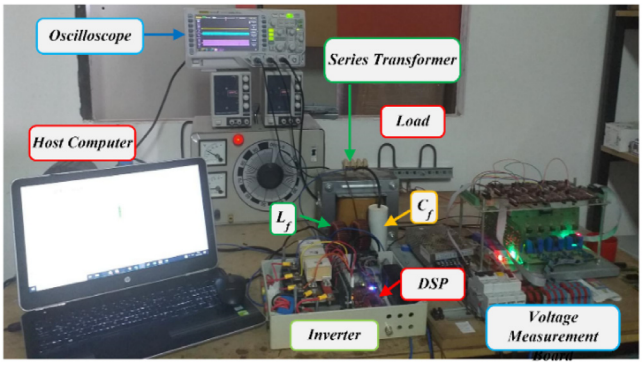

Fig. 6. Photograph of laboratory set up.

as a suitable tool to generate the reference voltage for the sliding mode controller proposed in Section 3.1.

Using the ESTF filtered states $\hat{\xi}_1$ and $\hat{\xi}_2$, the reference voltage (23) can be generated as:

$$V_L^{\star} = \mu \sin\left(\text{atan2}\left(\hat{\xi}_2, -\hat{\xi}_1\right)\right). \tag{53}$$

4. Simulation and experimental results

The effectiveness and feasibility of the proposed method have been verified by simulations and experiments. Simulations were carried out by MATLAB/Simulink. The experimental performance of the proposed CTSMC was observed in a real time environment. Laboratory setup used in this work is given in Fig. 6. The used parameters are given in Table 1. In the developed control methods, there are 5 positive constant parameters to tune. Parameters $\lambda_1 - \lambda_3$ are related to the CTSM controller while parameters λ_4 and λ_5 are related to the ESTF, which is the reference signal generation method. Control parameters need to satisfy the condition $\lambda_1 > \lambda_2 > \lambda_3 > \varpi^+$, i.e., the parameters need to be higher than the upper bound imposed on the external disturbance. Based on the disturbance term given by Eq. (8) and knowledge of

Table 1
Parameters for experimental study.

System and control parameters	Values
CTSMC gains	$\lambda_1 = 20000,\ \lambda_2 = 16000,\ \lambda_3 = 8000$
SP-ESTF gains	$\lambda_4 = \sqrt{2}\omega_n,\ \lambda_5 = 10,\ \tau = 5$ ms.
Grid voltage V_g and f_g	120 V (rms) 50 Hz
Grid impedance	$R_g = 1$ mΩ, $L_g = 0.1$ μH
Transformer turns ratio	1 : 1
DC link voltage, V_{dc}	120 V
LC filter	$L_f = 0.8$ mH, $C_f = 50$ μF
Sensitive series load	$R = 100$ Ω

Table 2
Qualitative comparative analysis of the methods considered in Section 5.

Control method	Tracking accuracy	THD
This Work	High	Very Low
ST-SMC (Biricik et al., 2021)	Medium	Medium
(a) Comparative analysis of control methods		
Filtering Method	THD	Frequency Estimation Harmonic Robustness
SP-STF	Low	High
ESTF	Very Low	High
SOGI-FLL (Rodríguez et al., 2011)	Medium	Low
(b) Comparative analysis of filtering methods		

DVR circuit, we have obtained the controller gains through trial and error. For the ESTF, the gain λ_4 is selected as a trade-off between fast convergence and harmonic disturbance rejection properties. By comparing the transfer function given by Eq. (33) with that of the standard second-order transfer function, one can find that for an optimal damping ratio of $1/\sqrt{2}$, the gain λ_4 should be selected as $\sqrt{2}\omega_n$ with ω_n being the nominal grid frequency. The gain λ_5 determines the grid frequency estimation accuracy. Through Eq. (42), one can see that this term determines the exponential convergence rate of the frequency estimation error. Through numerical simulation $\lambda_5 = 10$ has been found to provide a good comprise between the estimation accuracy and the convergence time.

The simulation results of the sag condition test are presented in Figs. 7 (a) and experimental results is presented in Figs. 7 (b) and (c). Captured wave-forms in Fig. 7 shows dynamic response of the DVR under 50% voltage sag in the grid voltage. As can be seen in both simulation and experimental results, the grid voltage is reduced from 120 V to 60 V. It can be seen that the converter of the DVR did not inject voltage before the sag occurs. During the sag condition at the grid voltage, the required voltage is generated by the converter and injected to the PCC. As a result of this injection, the voltage at the load terminals is almost not affected from the voltage sag.

The proposed controller's performance has also been tested in the case of voltage swell. For this case, the grid voltage was increased by 20% from 120 V to 144 V with the help of an auto-transformer. The simulation results are given in Fig. 8(a) and experimental test results are presented in Figs. 8 (b) and (c). Whether the grid voltage is increased or restored, the DVR injects the required voltage to the PCC and as a result load voltage was not affected by this adverse situation.

The response of the system during voltage fluctuations including harmonic distortion has been simulated and experimentally investigated. The simulation results in Fig. 9(a) and Experimental results in Fig. 9(b) and (c) show that the distorted grid voltage is successfully filtered at the load terminal.

5. Comparative simulation study

In this Section, simulation-based comparative studies are presented. As a comparison method, recently proposed ST-SMC (Biricik et al., 2021) has been chosen. It should be noted here that the CTSM controller considered in this work is a combination of both super twisting

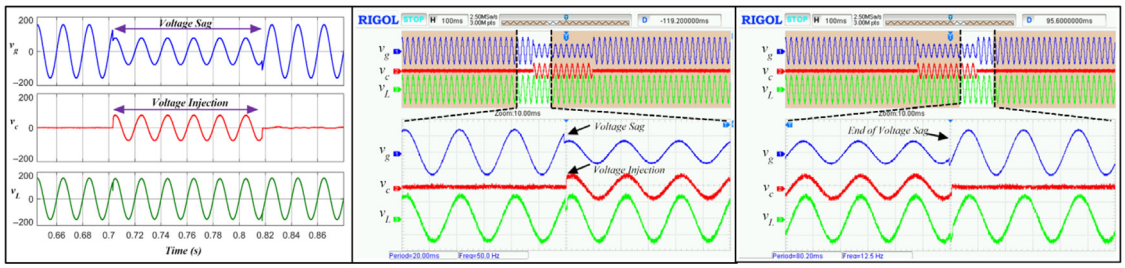

Fig. 7. Simulated and experimental responses of v_g, v_c, and v_L during voltage sag in the grid voltage, (a) Simulation, (b) and (c) Experiment.

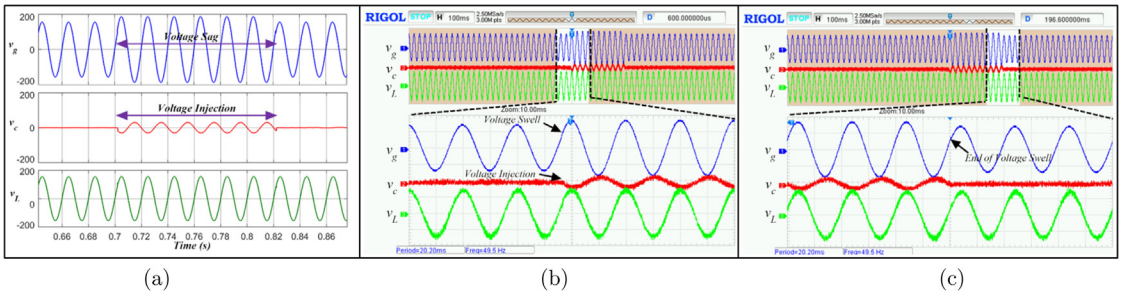

Fig. 8. Simulated and experimental responses of v_g, v_c, and v_L during voltage swell in the grid voltage, (a) Simulation, (b) and (c) Experiment.

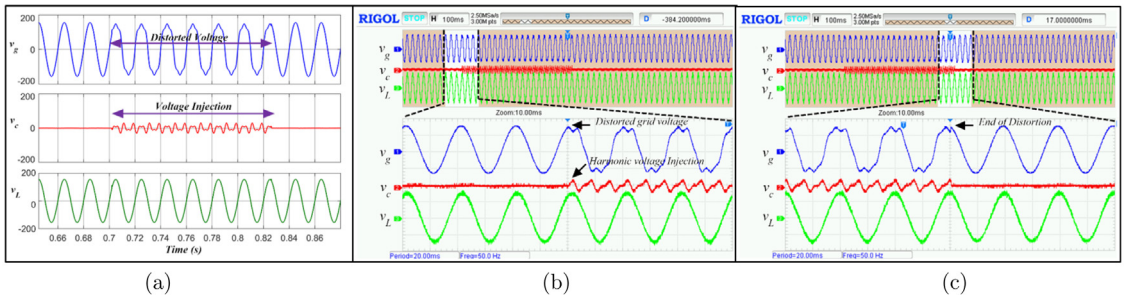

Fig. 9. Simulated and experimental responses of v_g, v_c, and v_L under harmonic distortions in the grid voltage, (a) Simulation, (b) and (c) Experiment.

Table 3
Comparisons with the existing wider literature on control of single-phase DVR.

Category	Hafezi and Faranda (2017)	Trabelsi et al. (2018)	Kumar and Mishra (2015)	Babaei, Kangarlu, and Sabahi (2010)	Bae, Lee, Jeong, and Han (2010)	Biricik and Komurcugil (2016)	Proposed
Topology	H-bridge	PUC	H-bridge	1ϕ-AC/AC	H-bridge	H-bridge	H-bridge
AC Current Sensor	2 i_L, i_{if}	2 i_f, i_g	2 i_s, i_f	0	2 v_g, v_L	0	0
AC Voltage Sensor	1 v_g	3 v_g, V_1, V_2	2 v_g, v_c	2 v_g, v_c	2 i_s, i_L	2 v_g, v_c	2 v_g, v_c
Voltage Controller	PI	MPC	MPC	Rule-based	PD	SMC	CSMC
Parameter Insensitive	×	×	×	×	×	✓	✓
Controller Convergence	Asymptotic	Asymptotic	Asymptotic	No Info.	Asymptotic	Asymptotic	Finite-Time
Controller Complexity	Low	Medium	Medium	Medium	Low	Medium	Medium
Grid-Synchronization	PLL	PLL	PLL	×	PLL	None	ESTF
Harmonic Robustness	×	×	×	×	✓	×	✓

and terminal sliding control algorithms. As such, the CTSM controller can be considered as a fast convergent extension of the super twisting algorithm. For both techniques, the proposed single-phase ESTF has been selected as the reference generator to ensure fair comparison. In the simulation, suddenly the grid experiences a −50% voltage sag together with both low and high-order harmonics. The considered grid has a total harmonic distortion (THD) of 14.7% and the individual harmonic components are: 3rd − 10%, 5th − 8%, 9th − 6%, and 13th − 4%.

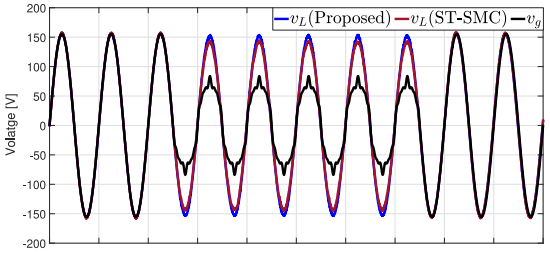

(a) Grid and load voltages.

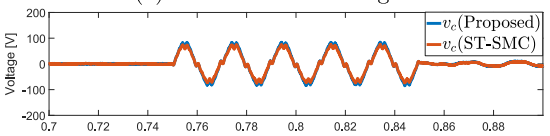

(b) DVR output voltage.

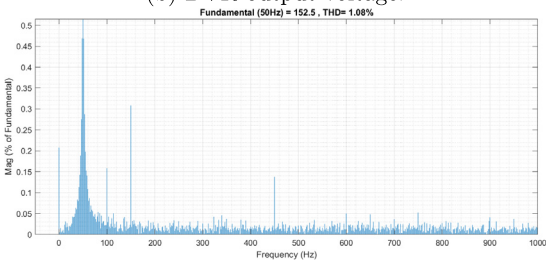

(c) Load voltage distortion by the proposed controller.

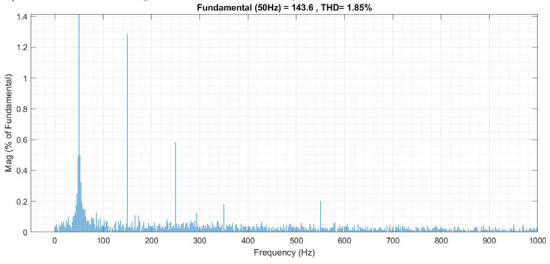

(d) Load voltage distortion by the ST-SMC.

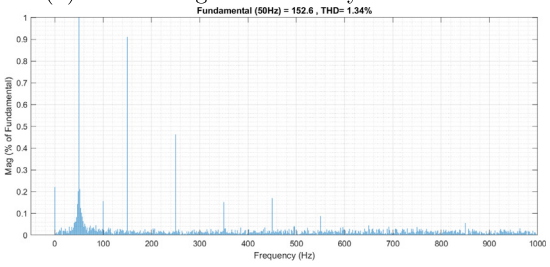

(e) Load voltage distortion with SP-STF.

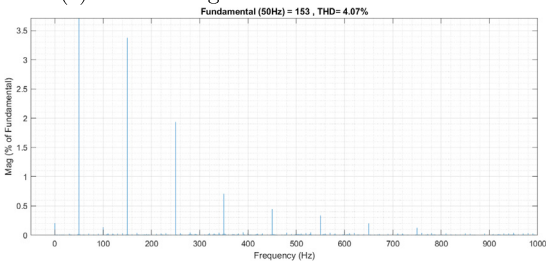

(e) Load voltage distortion with SOGI-FLL.

Fig. 10. Comparative simulation results.

Comparative simulation results given in Fig. 10(a) show that despite the change in the grid voltage, the load voltage remained constant by the proposed controller, however, ST-SMC controller has higher tracking error in the presence of voltage sag and distortion. Higher tracking error is evidenced by the DVR output voltage in Fig. 10 (b). Using the CTSM method, a THD of 1.08% has been achieved while it is 1.85% for the super twisting counterpart. This represents a significant reduction in the THD of the load voltage, which results in higher efficiency and lower energy consumption by the DVR. High distortion can enhance the degradation of insulation materials in electrical equipment (Caramia et al., 2000). As such, the proposed method can significantly enhance the lifetime of DVR and the load by reducing the THD compared to the existing ST-SMC approach. The results in Section 5 show the suitability of the proposed technique over ST-SMC.

In this work, two filters are proposed, namely SP-STF and ESTF. ESTF is an extension of SP-STF and is proposed by keeping in mind the harmonic robustness. As a comparison filter, SOGI-FLL (Rodríguez et al., 2011) is selected. SOGI-FLL is undoubtedly one of the most popular single-phase grid synchronization techniques available in the literature. These three filters are tested using the same condition as above-described. For testing SP-STF and SOGI-FLL, CTSM is used as the DVR controller to ensure fair comparison among the filters. Load voltage THD when the proposed controller is used with SP-STF and SOGI-FLL-based reference generators are given in Fig. 10 (e) and (f). Results in Section 5 show that the proposed SP-STF filter achieves a THD of 1.34% while it is roughly 4% for the SOGI-FLL, which is the comparison method. Results show that the THD for SOGI-FLL is approximately 4 times higher compared to the ESTF, which is developed in this work. In addition, thanks to the double-stage filtering, the ESTF achieves 25% reduction in THD compared to the SP-STF, which uses single-stage filtering and is also developed in this work. These results highlight the advantage of ESTF and/or SP-STF as the reference generator tool for single-phase DVR application. A qualitative comparison between the comparative techniques can be found in Table 2.

A table-based comparison of the proposed technique with the wider literature is given Table 3.

6. Conclusion

In this paper, a continuous terminal sliding mode controller is applied to the dynamic voltage restorer for power quality improvement. To facilitate the reference compensation voltage generation for the controller, an enhanced single-phase self-tuning filter-type grid-synchronization strategy is also proposed. A delay-based linear regression framework is used to make the filter frequency-adaptive. Thanks to the continuous control signal, the proposed controller significantly eliminates the chattering while at the same time maintains fast dynamic performance. This also helps to achieve constant PWM switching frequency for the voltage source inverter. It has been demonstrated that the proposed grid-synchronization technique is highly capable of extracting the fundamental component even in heavily distorted grid conditions. Stability analysis of the controller and the filter are presented. All the theoretical developments are verified through experimental study by considering challenging grid voltage scenarios. Experimental results show that the proposed technique is very effective to maintain the desired load voltage even in the case of grid voltage sag/swell and distortions. As a future work, application of the proposed control method for DVR in improving the power quality of grid-connected and/or islanded microgrids can be considered.

CRediT authorship contribution statement

Hafiz Ahmed: Conception and design, Analysis and interpretation of the data, Writing – orginal draft, Writing – review & editing. **Samet Biricik:** Conception and design, Analysis and interpretation of the data, Writing – orginal draft, Writing – review & editing. **Hasan Komurcugil:** Conception and design, Analysis and interpretation of the data, Writing – orginal draft, Writing – review & editing. **Seifeddine Ben Elghali:** Conception and design, Analysis and interpretation of the data, Writing – orginal draft, Writing – review & editing. **Mohamed Benbouzid:** Conception and design, Analysis and interpretation of the data, Writing – orginal draft, Writing – review & editing.

Declaration of competing interest

The authors declare that they have no known competing financial interests or personal relationships that could have appeared to influence the work reported in this paper.

Acknowledgments

All authors approved version of the manuscript to be published.

References

Abdusalam, M., Poure, P., Karimi, S., & Saadate, S. (2009). New digital reference current generation for shunt active power filter under distorted voltage conditions. *Electric Power Systems Research*, *79*(5), 759–765.

Ahmed, H. (2015). Reactive power and voltage control in grid-connected wind farms: an online optimization based fast model predictive control approach. *Electrical Engineering*, *97*(1), 35–44.

Ahmed, H., & Benbouzid, M. (2020a). Demodulation type single-phase PLL with DC offset rejection. *Electronics Letters*, *56*(7), 344–347.

Ahmed, H., & Benbouzid, M. (2020b). On the enhancement of generalized integrator-based adaptive filter dynamic tuning range. *IEEE Transactions on Instrumentation and Measurement*, *69*(10), 7449–7457. http://dx.doi.org/10.1109/TIM.2020.2982232.

Ahmed, H., Pay, M. L., Benbouzid, M., Amirat, Y., & Elbouchikhi, E. (2020). Gain normalized adaptive observer for three-phase system. *International Journal of Electrical Power & Energy Systems*, *118*, Article 105821.

Ahmed, H., Ríos, H., Ayalew, B., & Wang, Y. (2018). Second-order sliding-mode differentiators: an experimental comparative analysis using Van der Pol oscillator. *International Journal of Control*, *91*(9), 2100–2112.

Ahmed, H., Ushirobira, R., & Efimov, D. (2021). A simple frequency estimator for power systems. *IEEE Transactions on Instrumentation and Measurement*, *70*, 1–2. http://dx.doi.org/10.1109/TIM.2021.3094249.

Ahmed, H., Ushirobira, R., & Efimov, D. (2022). On biased harmonic signal estimation: Application to electric power grid monitoring. *IEEE Transactions on Control Systems Technology*, 1–8. http://dx.doi.org/10.1109/TCST.2022.3155322.

Al Hosani, K., Nguyen, T. H., & Al Sayari, N. (2018). An improved control strategy of 3P4W DVR systems under unbalanced and distorted voltage conditions. *International Journal of Electrical Power & Energy Systems*, *98*, 233–242.

Babaei, E., Kangarlu, M. F., & Sabahi, M. (2010). Compensation of voltage disturbances in distribution systems using single-phase dynamic voltage restorer. *Electric Power Systems Research*, *80*(12), 1413–1420.

Bae, B., Lee, J., Jeong, J., & Han, B. (2010). Line-interactive single-phase dynamic voltage restorer with novel sag detection algorithm. *IEEE Transactions on Power Delivery*, *25*(4), 2702–2709.

Biricik, S., Khadem, S. K., Redif, S., & Basu, M. (2018). Voltage distortion mitigation in a distributed generation-integrated weak utility network via a self-tuning filter-based dynamic voltage restorer. *Electrical Engineering*, *100*(3), 1857–1867.

Biricik, S., & Komurcugil, H. (2016). Optimized sliding mode control to maximize existence region for single-phase dynamic voltage restorers. *IEEE Transactions on Industrial Informatics*, *12*(4), 1486–1497.

Biricik, S., Komurcugil, H., Ahmed, H., & Babaei, E. (2021). Super twisting sliding mode control of DVR with frequency-adaptive brockett oscillator. *IEEE Transactions on Industrial Electronics*, *68*(11), 10730–10739. http://dx.doi.org/10.1109/TIE.2020.3038089.

Biricik, S., Komurcugil, H., Tuyen, N. D., & Basu, M. (2019). Protection of sensitive loads using sliding mode controlled three-phase DVR with adaptive notch filter. *IEEE Transactions on Industrial Electronics*, *66*(7), 5465–5475.

Biricik, S., Redif, S., Özerdem, Ö. C., Khadem, S. K., & Basu, M. (2014). Real-time control of shunt active power filter under distorted grid voltage and unbalanced load condition using self-tuning filter. *IET Power Electronics*, *7*(7), 1895–1905.

Caramia, P., Carpinelli, G., Verde, P., Mazzanti, G., Cavallini, A., & Montanari, G. (2000). An approach to life estimation of electrical plant components in the presence of harmonic distortion. In *Ninth International conference on harmonics and quality of power. proceedings (Cat. No.00EX441), vol. 3* (pp. 887–892). http://dx.doi.org/10.1109/ICHQP.2000.896846.

Çelik, D. (2022). Lyapunov based harmonic compensation and charging with three phase shunt active power filter in electrical vehicle applications. *International Journal of Electrical Power & Energy Systems*, *136*, Article 107564.

Çelik, D., & Meral, M. E. (2019). Current control based power management strategy for distributed power generation system. *Control Engineering Practice*, *82*, 72–85.

Chedjara, Z., Massoum, A., Massoum, S., Wira, P., Safa, A., & Gouichiche, A. (2018). A novel robust PLL algorithm applied to the control of a shunt active power filter using a self tuning filter concept. In *2018 IEEE International conference on industrial technology* (pp. 1124–1131). IEEE.

Cruz-Zavala, E., Moreno, J. A., & Fridman, L. M. (2011). Uniform robust exact differentiator. *IEEE Transactions on Automatic Control*, *56*(11), 2727–2733. http://dx.doi.org/10.1109/TAC.2011.2160030.

Dao, T., Biricik, S., & Ngo, T. (2020). A comprehensive analysis of grid synchronization systems for power converters. In *IECON 2020 the 46th Annual conference of the ieee industrial electronics society* (pp. 4935–4940).

Ding, L., Han, Q.-L., & Ning, B. (2022). *Distributed control and optimization of networked microgrids: A multi-agent system based approach*. Springer Nature.

Ding, L., Han, Q.-L., Ning, B., & Yue, D. (2020). Distributed resilient finite-time secondary control for heterogeneous battery energy storage systems under denial-of-service attacks. *IEEE Transactions on Industrial Informatics*, *16*(7), 4909–4919. http://dx.doi.org/10.1109/TII.2019.2955739.

Falehi, A. D., & Torkaman, H. (2021). Promoted supercapacitor control scheme based on robust fractional-order super-twisting sliding mode control for dynamic voltage restorer to enhance FRT and PQ capabilities of DFIG-based wind turbine. *Journal of Energy Storage*, *42*, Article 102983.

Fridman, L., Moreno, J. A., Bandyopadhyay, B., Kamal, S., & Chalanga, A. (2015). Continuous nested algorithms: The fifth generation of sliding mode controllers. In *Recent advances in sliding modes: from control to intelligent mechatronics* (pp. 5–35). Springer.

Gautam, S., Xiao, W., Lu, D. D.-C., Ahmed, H., & Guerrero, J. M. (2022). Development of frequency-fixed all-pass filter based single-phase phase-locked loop. *IEEE Journal of Emerging and Selected Topics in Power Electronics*, *10*(1), 506–517. http://dx.doi.org/10.1109/JESTPE.2021.3085124.

Hafezi, H., & Faranda, R. (2017). Dynamic voltage conditioner: A new concept for smart low-voltage distribution systems. *IEEE Transactions on Power Electronics*, *33*(9), 7582–7590.

(1998). IEEE recommended practice for evaluating electric power system compatibility with electronic process equipment. *IEEE Std 1346-1998*, http://dx.doi.org/10.1109/IEEESTD.1998.87816.

Kim, H., & Sul, S.-K. (2005). Compensation voltage control in dynamic voltage restorers by use of feed forward and state feedback scheme. *IEEE Transactions on Power Electronics*, *20*(5), 1169–1177.

Komurcugil, H., Biricik, S., Bayhan, S., & Zhang, Z. (2021). Sliding mode control: Overview of its applications in power converters. *IEEE Industrial Electronics Magazine*, *15*(1), 40–49. http://dx.doi.org/10.1109/MIE.2020.2986165.

Kumar, C., & Mishra, M. K. (2015). Predictive voltage control of transformer-less dynamic voltage restorer. *IEEE Transactions on Industrial Electronics*, *62*(5), 2693–2697.

Li, Y. W., Blaabjerg, F., Vilathgamuwa, D. M., & Loh, P. C. (2007). Design and comparison of high performance stationary-frame controllers for DVR implementation. *IEEE Transactions on Power Electronics*, *22*(2), 602–612.

Malathi, S., & Jayachandran, J. (2020). FPGA implementation of NN based LMS–LMF control algorithm in DSTATCOM for power quality improvement. *Control Engineering Practice*, *98*, Article 104378.

Moghassemi, A., & Padmanaban, S. (2020). Dynamic voltage restorer (DVR): a comprehensive review of topologies, power converters, control methods, and modified configurations. *Energies*, *13*(16), 4152.

Mukundan C. M., N., Naqvi, S. B. Q., Singh, B., & Jayaprakash, P. (2021). Single-layer decoupled multiple-order generalized integral control for single-stage solar energy grid integrator with maximum power extraction. *IEEE Transactions on Industrial Informatics*, *17*(1), 100–109. http://dx.doi.org/10.1109/TII.2020.2981125.

Ning, B., Han, Q.-L., & Ding, L. (2020). Distributed secondary control of AC microgrids with external disturbances and directed communication topologies: A full-order sliding-mode approach. *IEEE/CAA Journal of Automatica Sinica*, *8*(3), 554–564.

Ning, B., Han, Q.-L., & Ding, L. (2021). Distributed finite-time secondary frequency and voltage control for islanded microgrids with communication delays and switching topologies. *IEEE Transactions on Cybernetics*, *51*(8), 3988–3999. http://dx.doi.org/10.1109/TCYB.2020.3003690.

Nirmal Mukundan, C. M., Naqvi, S. B. Q., Singh, Y., Singh, B., & Jayaprakash, P. (2021). A cascaded generalized integral control for multiobjective grid-connected solar energy transfer system. *IEEE Transactions on Industrial Electronics*, *68*(12), 12385–12395. http://dx.doi.org/10.1109/TIE.2020.3048316.

Omar, A. I., Aleem, S. H. A., El-Zahab, E. E., Algablawy, M., & Ali, Z. M. (2019). An improved approach for robust control of dynamic voltage restorer and power quality enhancement using grasshopper optimization algorithm. *ISA Transactions*, *95*, 110–129.

Ouchen, S., Benbouzid, M., Blaabjerg, F., Betka, A., & Steinhart, H. (2021). Direct power control of shunt active power filter using space vector modulation based on supertwisting sliding mode control. *IEEE Journal of Emerging and Selected Topics in Power Electronics*, *9*(3), 3243–3253. http://dx.doi.org/10.1109/JESTPE.2020.3007900.

Pandey, A., Agrawal, R., Mandloi, R. S., & Sarkar, B. (2017). Sliding mode control of dynamic voltage restorer by using a new adaptive reaching law. *Journal of the Institution of Engineers (India): Series B*, *98*(6), 579–589.

Pay, M. L., Cao, P., Sun, Y., & McCluskey, D. (2020). Luenberger observer based grid synchronization techniques for smart grid application. In *IECON 2020 the 46th Annual Conference of the IEEE Industrial Electronics Society* (pp. 4955–4960).

Rodríguez, P., Luna, A., Candela, I., Mujal, R., Teodorescu, R., & Blaabjerg, F. (2011). Multiresonant frequency-locked loop for grid synchronization of power converters under distorted grid conditions. *IEEE Transactions on Industrial Electronics*, *58*(1), 127–138.

Roncero-Sánchez, P., Acha, E., Ortega-Calderon, J. E., Feliu, V., & García-Cerrada, A. (2008). A versatile control scheme for a dynamic voltage restorer for power-quality improvement. *IEEE Transactions on Power Delivery*, *24*(1), 277–284.

Roselyn, J. P., Chandran, C. P., Nithya, C., Devaraj, D., Venkatesan, R., Gopal, V., et al. (2020). Design and implementation of fuzzy logic based modified real-reactive power control of inverter for low voltage ride through enhancement in grid connected solar PV system. *Control Engineering Practice*, *101*, Article 104494.

Safa, A., Berkouk, E. M., Messlem, Y., Chedjara, Z., & Gouichiche, A. (2018). A pseudo open loop synchronization technique for heavily distorted grid voltage. *Electric Power Systems Research*, *158*, 136–146.

Sasitharan, S., & Mishra, M. K. (2010). Constant switching frequency band controller for dynamic voltage restorer. *IET Power Electronics*, *3*(5), 657–667.

Singh, N., & Jain, S. K. (2019). TOIL and damped-SOGI control of quasi-Z-source inverter based grid-connected renewable-system. *Control Engineering Practice*, *90*, 267–284.

Toumi, T., Allali, A., Meftouhi, A., Abdelkhalek, O., Benabdelkader, A., & Denai, M. (2020). Robust control of series active power filters for power quality enhancement in distribution grids: Simulation and experimental validation. *ISA Transactions*, *107*, 350–359.

Trabelsi, M., Komurcugil, H., Refaat, S. S., & Abu-Rub, H. (2018). Model predictive control of packed u cells based transformerless single-phase dynamic voltage restorer. In *2018 IEEE international conference on industrial technology* (pp. 1926–1931). IEEE.

Vamja, R. V., & Mulla, M. A. (2022). Reduced DC sensor based grid-interactive operation of single-stage solar photovoltaic water pumping system. *Energy Sources, Part A: Recovery, Utilization, and Environmental Effects*, 1–16.

Verma, A. K., Subramanian, C., & Jarial, R. K. (2022). An error demodulation technique for single-phase grid synchronization/LVRT applications. *IEEE Systems Journal*, *16*(2), 2261–2264. http://dx.doi.org/10.1109/JSYST.2021.3062878.